



# Obrabotka metallov -

# Metal Working and Material Science

Journal homepage: [http://journals.nstu.ru/obrabotka\\_metallov](http://journals.nstu.ru/obrabotka_metallov)



## Influence of hydrogen saturation on the structure and mechanical properties of Fe-17Cr-13Ni-3Mo-0.01C austenitic steel during rolling at different temperatures

Evgeny Melnikov<sup>a, \*</sup>, Galina Maier<sup>b</sup>, Valentina Moskvina<sup>c</sup>, Elena Astafurova<sup>d</sup>

Institute of Strength Physics and Materials Science of Siberian Branch of Russian Academy of Sciences, 2/4 pr. Akademicheskii, Tomsk, 634055, Russian Federation

<sup>a</sup>  <https://orcid.org/0000-0001-8238-6055>,  [melnickow-jenya@yandex.ru](mailto:melnickow-jenya@yandex.ru), <sup>b</sup>  <https://orcid.org/0000-0003-3043-9754>,  [galinazg@yandex.ru](mailto:galinazg@yandex.ru),  
<sup>c</sup>  <https://orcid.org/0000-0002-6128-484X>,  [valya\\_moskvina@mail.ru](mailto:valya_moskvina@mail.ru), <sup>d</sup>  <https://orcid.org/0000-0002-1995-4205>,  [elena.g.astafurova@ispms.ru](mailto:elena.g.astafurova@ispms.ru)

### ARTICLE INFO

#### Article history:

Received: 15 February 2021

Revised: 09 March 2021

Accepted: 29 March 2021

Available online: 15 June 2021

#### Keywords:

Austenitic steel

Plastic deformation

Hydrogenization

Microstructure

Mechanical properties

#### Funding

The work was carried out within the framework of the state assignment of the IPPM SB RAS, topic number FWRW-2019-0030.

#### Acknowledgements

The studies were carried out on the equipment of IPPM SB RAS (Center for Collective Use “Nanotech”) and NRU “BelGU” (Center for Collective Use “Diagnostics of the structure and properties of nano-materials”).

### ABSTRACT

**Introduction.** The development of hydrogen energy implies a decrease in the dependence of various human activities on fossil energy sources and a significant reduction in carbon dioxide emission into the atmosphere. Therefore, the requirements for the quality of structural materials, which have the prospect of being used for storage and transportation of hydrogen, as well as for the creation of infrastructure facilities for hydrogen energy, are increasing. Therefore, the scientific researches on the hydrogen-assisted microstructure and mechanical behavior of structural materials in various loading schemes are of great importance. **The aim of this work** is to establish the effect of chemical-deformation treatment, including rolling combined with hydrogen saturation, on the microstructure, phase composition, and mechanical properties of 316L-type austenitic stainless steel. **Methods.** Transmission electron microscopy and backscattered electron diffraction, X-ray diffraction, X-ray phase and magnetic phase analysis, microindentation and uniaxial static tension are utilized. **Results and Discussion.** It is shown experimentally that after rolling with 25 and 50 % upset, the morphology of the defect structure and the phase composition of 316L steel substantially depends on the deformation temperature (at room temperature or with the cooling of the samples in the liquid nitrogen) and on hydrogen saturation rate (for 5 hours at a current density of 200 mA/cm<sup>2</sup>). The main deformation mechanisms of the steel in rolling are slip, twinning, and microlocalization of plastic flow, which all provide the formation of ultrafine grain-subgrain structure in the samples. In addition, deformation-induced  $\epsilon$  and  $\alpha'$  martensitic phases are formed in the structure of the rolled samples. Regardless of the regime of chemical-deformation processing, grain-subgrain structures with a high density of deformation defects are formed in steel, but its morphologies are dependent on the processing regime. The experimental data indicate that both preliminary hydrogen saturation and a decrease in the deformation temperature contribute to the more active development of mechanical twinning and deformation-induced phase transformations during rolling. Despite the discovered effects on the influence of hydrogen saturation on the deformation mechanisms and the morphology of a defective microstructure formed during rolling, preliminary hydrogenation has little effect on the mechanical properties of steel at a fixed degree and temperature of deformation. These data indicate that irrespective of the morphology of the defective grain-subgrain structure, grain refinement, accumulation of deformation defects and an increase in internal stresses lead to an increase in the strength characteristics of the steel.

**For citation:** Melnikov E.V., Maier G.G., Moskvina V.A., Astafurova E.G. Influence of hydrogen saturation on the structure and mechanical properties of Fe-17Cr-13Ni-3Mo-0.01C austenitic steel during rolling at different temperatures. *Obrabotka metallov (tekhnologiya, oborudovanie, instrumenty)* = *Metal Working and Material Science*, 2021, vol. 23, no. 2, pp. 81–97. DOI: 10.17212/1994-6309-2021-23.2-81-97. (In Russian).

#### \* Corresponding author

Melnikov Evgeny V., Junior Researcher

Institute of Strength Physics and Materials,

Science of Siberian Branch of Russian Academy of Sciences,

2/4 pr. Akademicheskii,

634055, Tomsk, Russian Federation

Tel: 8 (3822) 28-68-65, e-mail: [melnickow-jenya@yandex.ru](mailto:melnickow-jenya@yandex.ru)

## Introduction

The development of methods and technologies gives reason to believe that hydrogen fuel cells will play an important role in energy production. Advances in hydrogen energy will help one to reduce the dependence on fossil fuels and significantly decrease carbon dioxide emission. Safe storage (ultrahigh-pressure tanks and containers) and transport of hydrogen (piping, valves, sleeves, springs, and gauges to regulate pressure) are key issues in the widespread using of hydrogen energy. In this regard, the requirements grow for the quality and service properties of structural materials that are exposed to hydrogen [1–3]. One of the important areas of research in this field is the evaluation of the mechanical behavior of structural materials subjected to hydrogen exposure under various loading conditions.

Austenitic stainless steels (SS) have good corrosion resistance and are less susceptible to hydrogen embrittlement than other steels [4, 5]. Therefore, such steels are candidate materials for various components of hydrogen transportation and storage systems. Cold plastic deformation of austenitic SS causes the formation of various types of deformation defects in the structure, and in some cases is accompanied by  $\gamma \rightarrow \epsilon$  and  $\gamma \rightarrow \alpha'$  phase transformations [6–13]. This leads to deformation and fragmentation of the grain structure and, consequently, to a change in the mechanical properties of steel under cold deformation (an increase in microhardness, a yield strength and an ultimate tensile strength, and a decrease in plasticity). The choice of materials for hydrogen energy should consider the effect of hydrogen as an alloying element on deformation-induced processes in austenitic stainless steels. Numerous works indicate that SS with high stability of austenite to phase transformations (for example, Fe-17Cr-14Ni-3Mo or Fe-18Cr-20Ni-2Si) are less susceptible to hydrogen embrittlement than steel grades with low stability (for example, Fe-18Cr-8Ni, Fe-18Cr-10Ni, Fe-18Cr-10Ni-Ti) [3, 5, 14–18]. The stability of austenitic SS to phase transformations depends on stacking fault energy (SFE), which is determined by the steel chemical composition [19–22]. At the same time, it is shown in [4] that not only deformation phase transformations, including those hydrogen-induced, cause hydrogen degradation of the mechanical properties of austenitic steels, but also the type of deformation-assisted dislocation arrangement. Stable steels with high SFE, in which a planar dislocation structure develops, are more susceptible to hydrogen embrittlement than those with wavy slip [4]. All above-mentioned studies indicate that hydrogen effectively affects both the type of microstructure and phase transformations in austenitic steels.

The steel of composition Fe-17Cr-13Ni-3Mo-0.01C (analog of AISI 316L) is a type of austenitic chromium-nickel stainless steel. It possesses high strain hardening rate, low tendency to deformation phase transformations at room temperature due to its high SFE [7, 10, 11, 19]. Despite the fact that the processes of hydrogen embrittlement for chromium-nickel steels with different SFE is studied in detail in uniaxial tension [3–5, 14–18, 23], there are almost no data on the effect of hydrogen on the structure refinement and hardening of these steels under other types of loading, for example, during rolling.

In this work, we investigated the effect of chemical-deformation processing regimes, including multipass rolling with preliminary saturation with hydrogen of the specimens, on phase composition, microstructure, deformation mechanisms and mechanical properties of Fe-17Cr-13Ni-3Mo-0.01C austenitic steel.

## Methods

The industrially melted stable austenitic stainless steel Fe-17Cr-13Ni-3Mo-0.01C is chosen as the material for investigation. The steel billets with the shape of the rectangular plates were cut using an electric spark machine. After cleaning in the aqua regia, the plates were kept at a temperature of 1100 °C for an hour and water-quenched at room temperature. Heat treatment was carried out in an inert gas (helium) environment. After heat treatment, the plates were mechanically ground and electrolytically polished in a solution of 25 g  $\text{CrO}_3$  + 210 ml  $\text{H}_3\text{PO}_4$ . Before hydrogen saturation, all plates had the same size of  $10 \times 20 \times 1 \text{ mm}^3$ .

The first portion of specimens was electrolytically hydrogen saturated for 5 hours at room temperature. Hydrogen saturation was carried out in 1N aqueous solution of sulfuric acid ( $\text{H}_2\text{SO}_4$ ) with add of

thiourea ( $\text{CH}_4\text{N}_2\text{S}$ ) at a current density  $j = 200 \text{ mA/cm}^2$ . Immediately after hydrogen saturation, the plates were rolled using two regimes: regime I – at room temperature ( $23 \text{ }^\circ\text{C}$ ), regime II – with cooling of the plates down to liquid nitrogen temperature ( $-196 \text{ }^\circ\text{C}$ ) before each rolling path. Plastic deformation per single pass through the rolls of the rolling mill was  $\approx 3\text{--}4 \%$ . The rolling reduction was calculated as  $e = ((h_0 - h_1)/h_0)100 \%$ , where  $h_0$  is the initial plate thickness (1 mm),  $h_1$  is the plate thickness after rolling. The total reduction was 25 and 50 %. The second portion of specimens was rolled using the identical regimes, but without preliminary saturation with hydrogen. Further in the text, the specimens after heat treatment (but non-deformed) are named as initial one.

The microhardness of the specimens was determined by the Vickers method on a Duramin 5 microhardness tester with a load on the indenter of 200 g. Uniaxial static tension was carried out on an Instron 3369 testing machine at room temperature with an initial strain rate of  $4.2 \times 10^{-4} \text{ s}^{-1}$ . Dumb-bell shaped flat tensile specimens were cut from the rolled plates. The tensile specimens had the dimensions of  $9 \times 2.6 \times h_1$  mm in gauge section.

X-ray phase and X-ray structural analyses (XRD) of phase composition and structural parameters of steel were carried out on a Rigaku Ultima IV diffractometer ( $\text{CuK}\alpha$  radiation). The calculation of a crystal lattice microstrain ( $\Delta d/d$ ) and the sizes of coherent scattering regions (CSR) were performed by the approximation method. The volume fraction of strain-induced  $\alpha'$ -martensite ( $V_{\alpha'}$ ) formed in specimens was determined by the measuring of a specific magnetization depending on magnetic field strength using a Magnetometer N-04 device (magnetic phase analysis, MFA) [26].

Electron microscopic studies of the specimens' structure were carried out using a JEM-2100 transmission electron microscope (TEM) at an accelerating voltage of 200 kV. Foils for TEM research were prepared by the standard method described in [27]. The dislocation density was calculated according to the procedure given in [27]. The grain size of the initial heat-treated billet was determined using the grain maps reconstructed from the electron backscattered diffraction (EBSD) data (a Quanta 200 3D scanning electron microscope, an accelerating voltage of 30 kV).

## Results and Discussion

### *XRD results*

Figure 1 shows the X-ray diffraction patterns obtained for steel specimens in the initial state and after various regimes of the chemical-deformation processing. According to XRD results, the initial austenitic structure of Fe-17Cr-13Ni-3Mo-0.01C steel possesses a lattice parameter  $a = 0.3603 \text{ nm}$ , microstrain of the crystal lattice –  $\Delta d/d = 7.3 \times 10^{-4}$  and CSR  $> 200 \text{ nm}$ .

X-ray phase analysis of steel specimens subjected to different regimes of chemical-deformation processing revealed the presence of  $\gamma$ -phase only. Thus, austenitic SS maintains a single-phase fcc crystal structure regardless of the processing regime (Fig. 1). XRD analysis indicates the deformation-induced refinement of the structure and the increase in internal stresses in the specimens. Regardless of the deformation temperature and hydrogen saturation, the microstrain of the crystal lattice increases after rolling up to  $1.5\text{--}2.9 \times 10^{-3}$ . Rolling significantly reduces CSR values (Table 1). The lattice parameter of austenite changes insignificantly after all processing regimes. It should be noted that at the same reduction in rolling, two factors – a decrease in the rolling temperature and preliminary saturation with hydrogen – promote the increase in CSR values in comparison with specimens rolled at room temperature and without preliminary saturation with hydrogen. This result indicates, first, a hydrogen-assisted and temperature-assisted change in the fragmentation of the microstructure and, probably, the deformation mechanisms in specimens during rolling. Second, these data indicate similar effect of both aforementioned factors on the microstructure of the steel during rolling.

A comparative analysis of the XRD patterns shows a decrease in the intensity and broadening of X-ray lines with an increase in the reduction (strain) (Fig. 1). During rolling, deformation texture of the  $\{220\}$  type is formed in the rolling plane, as it is illustrated by changing in the ratio of the X-ray lines intensi-

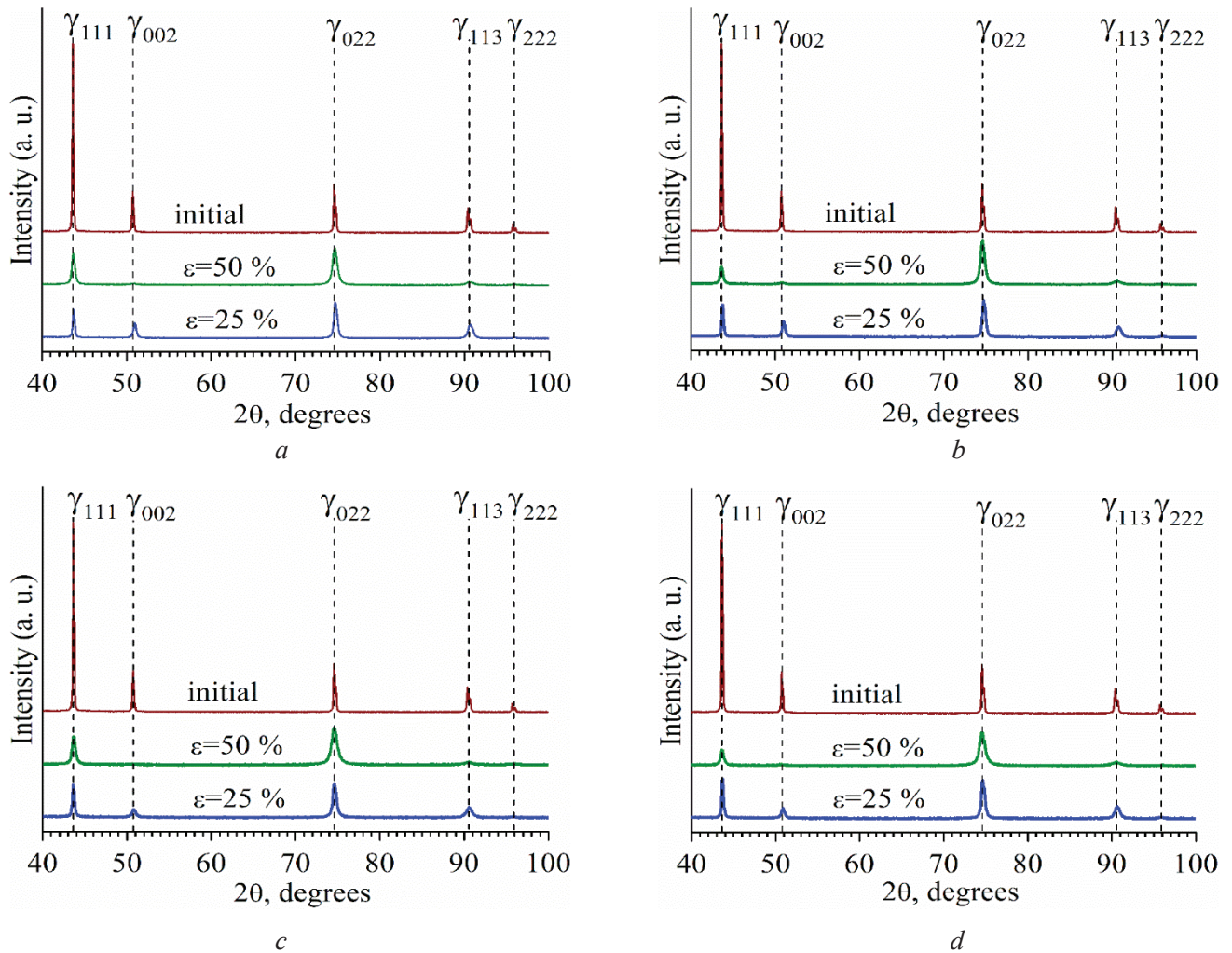


Fig. 1. XRD patterns for Fe-17Cr-13Ni-3Mo-0.01C steel in the initial state, after processing according to regime I (a, b) and regime II (c, d); a, c – rolling of hydrogen-free specimens; b, d– rolling of hydrogen saturated specimens. The reduction in rolling is shown in the figures

Table 1

**Relative intensities of XRD maxima, the ratios of intensities for 111 $\gamma$  and 022 $\gamma$  reflections and sizes of the coherent scattering regions (CSR) for Fe-17Cr-13Ni-3Mo-0.01C steel before and after chemical-deformation treatment**

| CDT                                 | 111 $\gamma$ | 002 $\gamma$ | 022 $\gamma$ | 113 $\gamma$ | $I_{111\gamma}/I_{022\gamma}$ | CSR, nm |
|-------------------------------------|--------------|--------------|--------------|--------------|-------------------------------|---------|
| initial                             | 100.00       | 20.67        | 26.76        | 13.50        | 3.74                          | >200    |
| Rolling without hydrogen saturation |              |              |              |              |                               |         |
| regime I, $\varepsilon = 25\%$      | 44.44        | 19.13        | 100.00       | 23.90        | 0.44                          | 11      |
| regime I, $\varepsilon = 50\%$      | 78.64        | 3.05         | 100.00       | 7.96         | 0.79                          | 7       |
| regime II, $\varepsilon = 25\%$     | 92.16        | 20.97        | 100.00       | 28.07        | 0.92                          | 44      |
| regime II, $\varepsilon = 50\%$     | 73.73        | 0.78         | 100.00       | 6.24         | 0.74                          | 30      |
| Rolling after hydrogen saturation   |              |              |              |              |                               |         |
| regime I, $\varepsilon = 25\%$      | 83.19        | 36.57        | 100.00       | 26.59        | 0.83                          | 14      |
| regime I, $\varepsilon = 50\%$      | 36.35        | 2.94         | 100.00       | 7.55         | 0.36                          | 7       |
| regime II, $\varepsilon = 25\%$     | 98.50        | 20.47        | 100.00       | 29.28        | 0.98                          | 70      |
| regime II, $\varepsilon = 50\%$     | 42.04        | 1.91         | 100.00       | 9.39         | 0.42                          | 40      |

ties (Fig. 1, Table 1). At 25 % reduction, that is, at early deformation degrees, hydrogen saturation and a decrease in the test temperature insignificantly suppress the formation of  $\{220\}$ -type texture in the rolling plane. With an increase in the reduction up to 50 %, over against, both these factors contribute a significant increase in the relative intensity of austenitic 220 $\gamma$  line in comparison with a lower strain (Table 1). Together with data on the change in CSR values, this may indicate the activation of deformation twinning and/or  $\gamma \rightarrow \epsilon$  deformation-induced transformation at low strains due to preliminary saturation with hydrogen and the decrease in the test temperature. Both these mechanisms contribute the formation of special boundaries  $\Sigma 3''$ , which inhibit dislocations motion, propagation of microshear bands, and impede the formation of a misoriented grain/subgrain structure with boundaries of general type [28–30]. As a result of the destruction of the grid of the special boundaries, which has been formed at small strains, the rolling texture is formed during subsequent rolling to 50 % reduction by analogy with specimens deformed without preliminary saturation with hydrogen (Fig. 1, Table 1).

### Results of transmission electron microscopic studies

The initial specimens have the homogeneous grain structure. The average grain size of austenite is 15  $\mu\text{m}$ , as it is determined by EBSD-maps. Chemical-deformation processing promotes significant grain refinement and the formation of a grain/subgrain structure with a high density of defects of the crystal structure (Figs. 2 and 3). The dislocation density increases from  $\sim 10^{12}$  to  $\sim 10^{15} \text{ m}^{-2}$  during rolling.

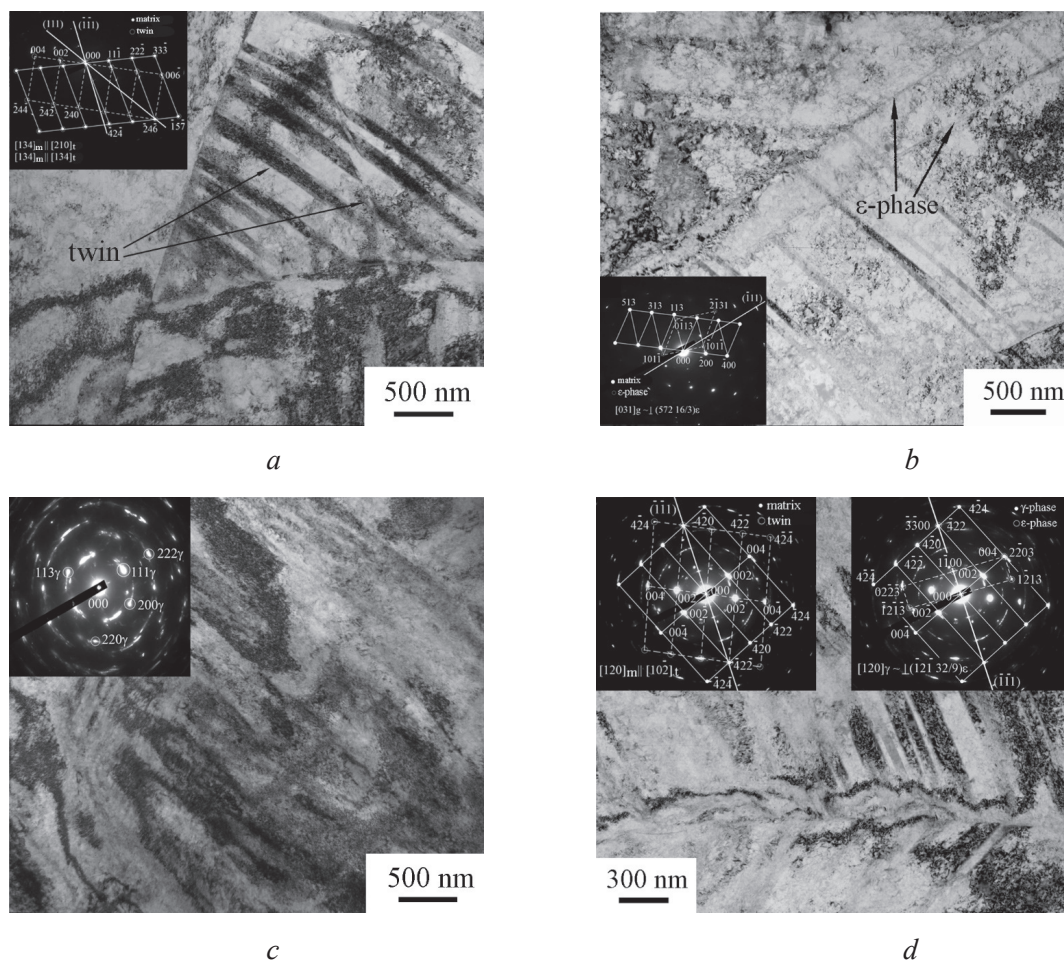


Fig. 2. TEM images of the microstructure in steel after processing in regime I:

*a, c* – rolling of hydrogen-free specimens; *b, d* – rolling of hydrogen-charged specimens. Reduction: 25% (*a, b*) and 50% (*c, d*). Selected area electron diffraction patterns are obtained from an area of  $1.4 \mu\text{m}^2$

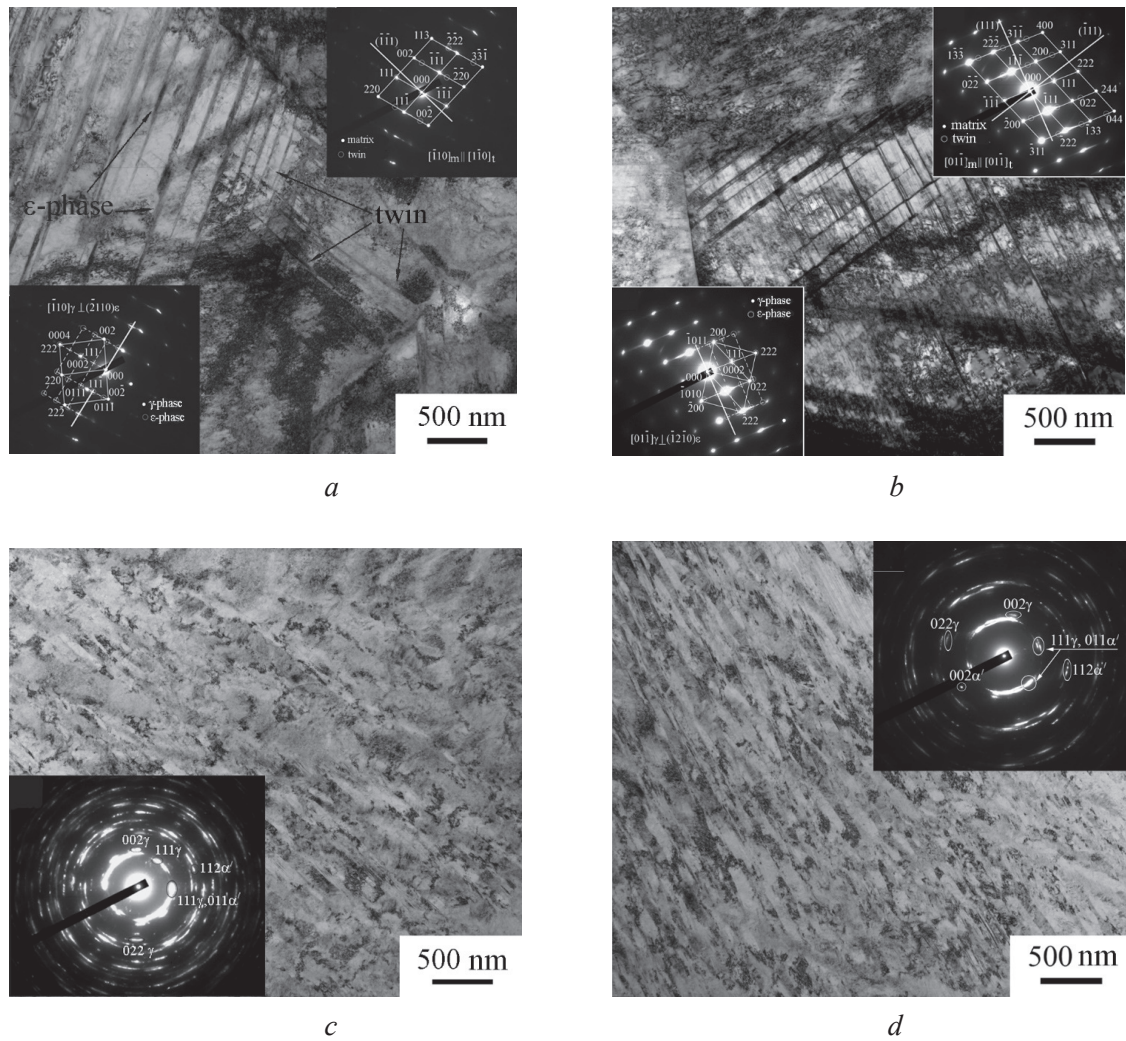


Fig. 3. TEM images of the microstructure in steel after processing by regime II: *a, c* – rolling of hydrogen-free specimens; *b, d* – rolling of hydrogen saturated specimens. Reduction: 25 % (*a, b*) and 50 % (*c, d*). Selected area electron diffraction patterns are obtained from an area of  $1.4 \mu\text{m}^2$

Figure 2 shows bright-field TEM images of the microstructure and the corresponding selected area electron diffraction patterns (inserts) for specimens rolled at room temperature (regime I). After rolling of specimens without preliminary saturation with hydrogen with  $\varepsilon = 25\%$ , the initial large austenitic grains are seen. The diffraction contrast inside of these grains testifies the accumulation of high dislocation density (Fig. 2, *a*, Table 2). Microdiffraction patterns for such a microstructure have a point character, with weak azimuthal diffusion of reflections. The dislocation arrangement indicates that the steel is characterized by “wavy” slip, typical for deformation of steels with medium-to-high SFE [31]. Both grains, in which deformation is realized due to slip only, and those with active slip and twinning are observed in TEM images. This is due to the orientation dependence of the twinning in austenitic steels [32, 33]. Under conditions of constrained deformation, the twinning stresses in Fe-17Cr-13Ni-3Mo-0.01C steel, which does not contain interstitial atoms, are not achieved in all grains, but in some grains this mechanism is realized. Twins with a thickness (lamella width)  $t = 50\text{--}100$  nm and with a distance between lamellas  $e = 60\text{--}100$  nm are frequently observed (Table 2). The linear density of twin boundaries in such grains is  $\rho_{t0} = 2 \times 10^6 \text{ m}^{-1}$  (Table 2). Rarely, individual grains are observed, in which the density of twin boundaries is higher than the average value ( $\rho_{t0} = 12 \times 10^6 \text{ m}^{-1}$ ). Obviously, these grains were most favorably oriented for the development of mechanical twinning (these grains possess the maximum Schmid factors for twinning).

The inhomogeneous grain/subgrain structure is formed after rolling with 50 % reduction (Fig. 2, *c*). Microdiffraction patterns contain numerous reflections of the austenite phase, distributed over the ring

Table 2

**Microstructure characteristics ( $\rho$  – dislocation density,  $t$  – twin thickness,  $e$  – distance between twins,  $\rho_{\text{tw}}$  – the linear density of twin boundaries) of steel microstructure after chemical-deformation processing**

| CDT                                 | $\rho$ , m <sup>-2</sup> | $t$ , nm                        | $e$ , nm                        | $\rho_{\text{tw}}$ , m <sup>-1</sup>        |
|-------------------------------------|--------------------------|---------------------------------|---------------------------------|---|
| Rolling without hydrogen saturation |                          |                                 |                                 |   |
| regime I, $\varepsilon = 25\%$      | $0.4 \times 10^{15}$     | 50–100<br>(15–25 <sup>*</sup> ) | 60–100<br>(15–40 <sup>*</sup> ) | $2 \times 10^6$<br>( $12 \times 10^{6*}$ )  |
| regime I, $\varepsilon = 50\%$      | $0.8 \times 10^{15}$     | 60–150<br>(15–30 <sup>*</sup> ) | 40–130<br>(20–40 <sup>*</sup> ) | $6 \times 10^6$<br>( $16 \times 10^{6*}$ )  |
| regime II, $\varepsilon = 25\%$     | $0.7 \times 10^{15}$     | 20–100                          | 50–150                          | $7 \times 10^6$                             |
| regime II, $\varepsilon = 50\%$     | $1.0 \times 10^{15}$     | 30–60                           | 30–60                           | $10 \times 10^6$                            |
| Rolling after hydrogen saturation   |                          |                                 |                                 |   |
| regime I, $\varepsilon = 25\%$      | $0.8 \times 10^{15}$     | 50–200 (20–50) <sup>*</sup>     | 70–250 (25–50 <sup>*</sup> )    | $8 \times 10^6$<br>( $29 \times 10^{6*}$ )  |
| regime I, $\varepsilon = 50\%$      | $1.2 \times 10^{15}$     | 50–100<br>(15–45 <sup>*</sup> ) | 50–150<br>(30–50 <sup>*</sup> ) | $13 \times 10^6$<br>( $34 \times 10^{6*}$ ) |
| regime II, $\varepsilon = 25\%$     | $0.8 \times 10^{15}$     | 10–60                           | 40–150                          | $30 \times 10^6$                            |
| regime II, $\varepsilon = 50\%$     | $1.5 \times 10^{15}$     | 10–40                           | 20–60                           | $40 \times 10^6$                            |

\* In individual grains that are favorably oriented for twinning.

(Fig. 2, *c*, insert). This indicates the formation of high-angle misorientations in the steel structure as a result of plastic deformation, while high azimuthal diffusions of the reflections confirm the presence of low-angle misorientations as well. Localized deformation bands (shear bands) of various scales are formed in rolling. Broken and separated twin boundaries are observed inside and between such bands (Fig. 2, *c*). Deformation twins are observed in most grains after 50 % reduction. The analysis of TEM images indicates the increase in the linear density of twin boundaries and the density of dislocations in comparison with the specimens rolled to 25 % reduction (Table 2).

Preliminary saturation with hydrogen before rolling promotes the development of deformation twinning, which leads to a significant increase in the linear density of twin boundaries in comparison with the structure after rolling in regime I without hydrogen saturation (Table 2, Fig. 2). Twinning is observed in almost all grains at 50 % reduction (Fig. 2, *d*). Mechanical twinning as a deformation mechanism is facilitated primarily due to a decrease in SFE of steel alloyed with hydrogen atoms. The formation of twins can be observed even in grains unfavorably oriented for this deformation mechanism [34, 35]. TEM studies also show the presence of thin  $\varepsilon$ -martensite lamellae inside of austenitic grains, but its amount is not high (Fig. 2, *b*, *d*). Since the  $\varepsilon$ -phase is not determined by XRD, its volume fraction is not above 5 %. The formation of the  $\varepsilon$ -phase also confirms the decrease in SFE of hydrogen-alloyed steel. After rolling up to 50 % reduction, diffraction patterns are predominantly point-like, although azimuthal diffusions of the reflections are present (Fig. 2, *d*, inserts). TEM studies have shown that preliminary saturation with hydrogen of the specimens before rolling contributes to the formation of a less misoriented structure relative to those deformed without preliminary saturation with hydrogen. This is obviously associated with the formation of a high density of special boundaries (twins and  $\varepsilon$ -phase). Along with the twinning, an increase in dislocation density is observed in comparison with specimens rolled to the similar reduction (strain) but without preliminary saturation with hydrogen (Table 2). This may be due to the hindered transfer of shear across twin boundaries and the accumulation of slip dislocations in the regions between special boundaries. Microstructural TEM studies confirm X-ray structural analysis data on the texture formation during rolling of the specimens, presented and discussed above. In terms of the special boundaries network formation, the microstructure of hydrogen saturated and rolled specimens is more uniform in comparison with one produced without preliminary saturation with hydrogen.

After low temperature deformation of hydrogen-free specimens (cooling of the plates before each rolling cycle, regime II), the details of its microstructure are quite similar to those deformed at room temperature after preliminary saturation with hydrogen (Figs. 2 and 3). A decrease in SFE of steel due to decrease in the deformation temperature is a well-known fact, and here it causes effect similar to alloying of the specimens with hydrogen before rolling.

Figure 3, *a* shows bright-field TEM image of microstructure and corresponding microdiffraction pattern (inserts) after rolling according to regime II without hydrogen saturation ( $\varepsilon = 25\%$ ). A decrease in the deformation temperature promotes the formation of the larger number of twins in the microstructure, thinner twin plates and shorter distances between it relative to the room-temperature deformation. This contributes to the increase in the linear density of twin boundaries (Table 2). Analysis of the diffraction pattern (Fig. 3, *a*, inserts show variants of interpretation of reflections corresponding to twins and the  $\varepsilon$ -phase) indicate that, in addition to twins in the austenite grains, plates of  $\varepsilon$ -martensite are observed. It ought to be noted that in deformation regime I,  $\varepsilon$ -martensite plates have been observed only after rolling with hydrogen saturation (Fig. 2, *b*).

Figure 3, *c* shows bright-field TEM image of misoriented grain/subgrain structure corresponded to the rolling of the steel in regime II with 50% reduction without preliminary saturation with hydrogen. Comparison of TEM images in Figures 2, *c* and 3, *c* indicates that, in contrast to deformation at room temperature, the cooling of the specimens is accompanied with the formation of a more homogeneous misoriented structure with deformation microbands, twins, and high density of dislocations (Table 2). Diffraction analysis of these specimens indicates the formation of  $\alpha'$ -phase in the structure. Selected area electron diffraction pattern has a quasi-ring character. It shows numerous austenitic reflections with high azimuthal diffusions, as well as reflections of  $\varepsilon$ - and  $\alpha'$ -deformation martensite (Fig. 3, *c*, insert). However, the fraction of  $\varepsilon$ - and  $\alpha'$ -phases is not high, since it is not identified by XRD (Fig. 1, *c*). According to magnetic phase analysis, the volume fraction of  $\alpha'$ -martensite in these specimens is  $V_{\alpha'} = 4.5\%$ .

In specimens after hydrogen saturation and rolling in regime II ( $\varepsilon = 25\%$ ), a homogeneous dense grid of twin boundaries is formed (Fig. 3, *b*). It consists of twin lamellae of 30–60 nm thick. Inside of this grid, there are even thinner twins of 10–15 nm thick and the density of twin boundaries reaches  $\rho_{tw} = 30 \times 10^6 \text{ m}^{-1}$  (Table 2). Selected area diffraction patterns show point reflections corresponding to  $\alpha'$ -phase, as well as reflections for  $\gamma$ -phase with strong azimuthal diffusions (Fig. 3, *d*, insert). In this case, the austenitic reflections do not form a quasi-ring pattern in contrast to that for the specimens rolled without hydrogen saturation (Fig. 3, *c*, insert). Magnetic phase analysis indicates that a deformation  $\alpha'$ -phase is also present in the specimens processed according to this regime, but its volume fraction is lower than that in specimens rolled without hydrogen saturation ( $V_{\alpha'} = 2.7\%$ ). This experimental fact requires further detailed research and analysis in a separate publication.

The realization of phase transformations, deformation microscopical localization (shear bands), high linear density of twin boundaries and dislocations after chemical-deformation processing by regime II all contribute to intensive grain refinement and formation of more uniform grain/subgrain structure in comparison with that in specimens subjected to processing in regime I. Preliminary saturation with hydrogen of austenitic SS and decrease in the deformation temperature both facilitate high density of twin boundaries in the microstructure of the specimens in this case.

### *Tensile test results*

Fig. 4 shows “stress-elongation” diagrams obtained by uniaxial static tension of the specimens processed according to different chemical-deformation regimes. The mechanical properties determined from these diagrams (elongation ( $\delta$ ), yield strength ( $\sigma_{0.2}$ ) and ultimate tensile strength ( $\sigma_b$ )) are summarized in Table 3.

In Fig. 4, curve 1 demonstrates the tensile diagram of the initial coarse-grained specimen (without any deformation pre-treatments). At the initial state steel possesses high ductility ( $\approx 63\%$ ) and low values of the yield strength ( $\sigma_{0.2} = 370 \text{ MPa}$ ) and ultimate tensile strength ( $\sigma_b = 660 \text{ MPa}$ ). Chemical-deformation processing leads to an increase in microhardness, a significant increase in strength properties and a decrease in

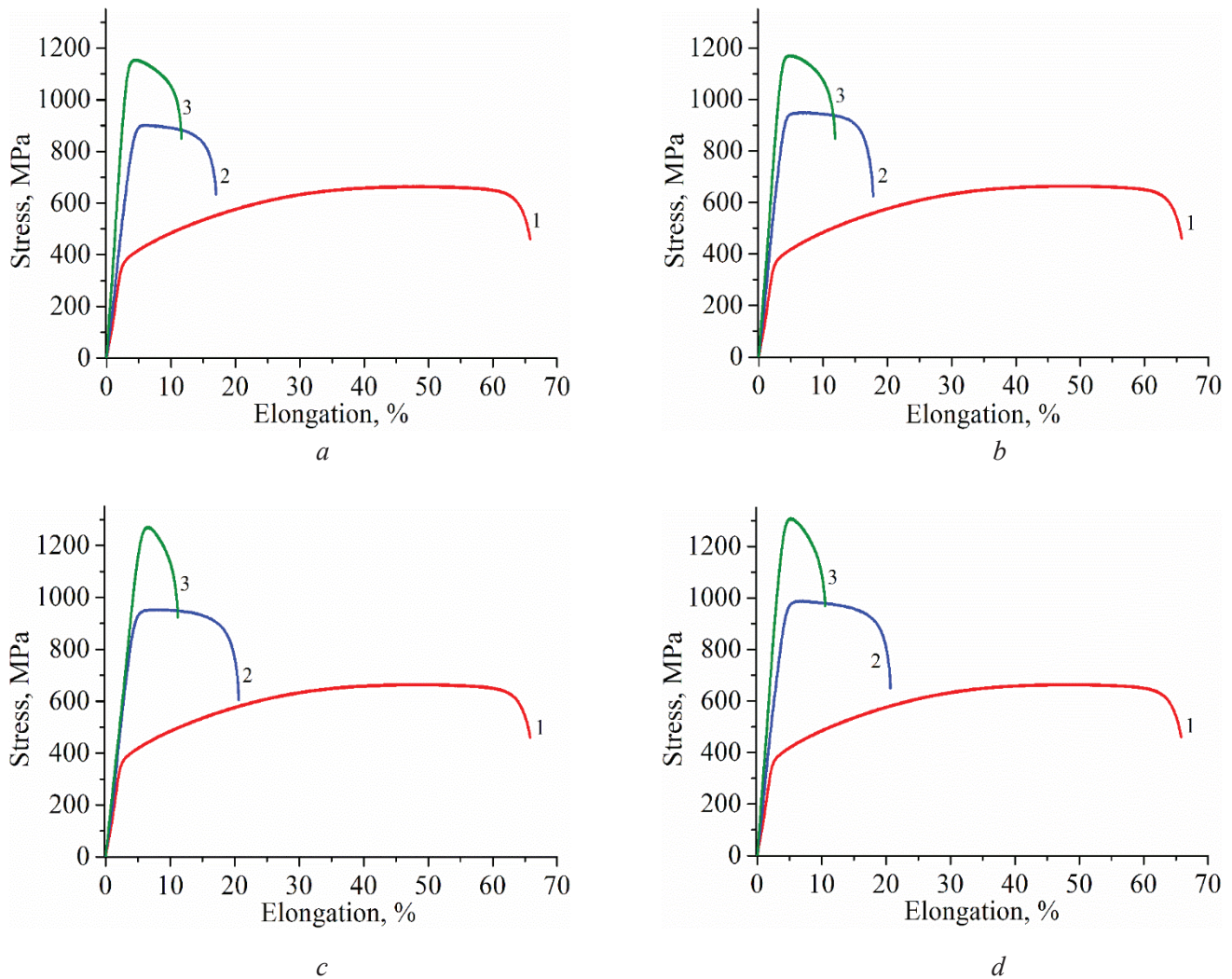


Fig. 4. Tensile diagrams of the initial (curve 1) steel specimens and those treated according to regime I (a, b) and regime II (c, d) (curve 2 –  $\epsilon=25\%$  and curve 3 –  $\epsilon=50\%$ ); a, c – after rolling of hydrogen-free specimens; b, d – after hydrogen saturation and rolling

Table 3

**The mechanical properties of Fe-17Cr-13Ni-3Mo-0.01C steel in the initial state and after chemical-deformation processing**

| CDT                                 | $\sigma_{0.2}$ , MPa | $\sigma_B$ , MPa | $\delta$ , % | $H\mu$ , GPa |
|-------------------------------------|----------------------|------------------|--------------|--------------|
| initial                             | 370                  | 660              | 63           | 2.17         |
| Rolling without hydrogen saturation |                      |                  |              |              |
| regime I, $\epsilon = 25\%$         | 830                  | 900              | 14           | 3.18         |
| regime I, $\epsilon = 50\%$         | 1110                 | 1150             | 9            | 3.53         |
| regime II, $\epsilon = 25\%$        | 850                  | 950              | 18           | 3.27         |
| regime II, $\epsilon = 50\%$        | 1230                 | 1270             | 7            | 3.97         |
| Rolling after hydrogen saturation   |                      |                  |              |              |
| regime I, $\epsilon = 25\%$         | 910                  | 950              | 15           | 3.31         |
| regime I, $\epsilon = 50\%$         | 1120                 | 1170             | 9            | 3.92         |
| regime II, $\epsilon = 25\%$        | 950                  | 990              | 18           | 3.42         |
| regime II, $\epsilon = 50\%$        | 1230                 | 1300             | 7            | 4.19         |

plasticity of the steel (Table 3). Depending on processing regime, the values of the yield strengths increase by factor of 2.5–2.6 and ultimate strength by factor of 1.4–1.6, while elongation to fracture decreases drastically (Table 3). When the yield point is reached in specimens subjected to chemical-deformation processing with 50% reduction, bands of localized plastic deformation are formed and a neck is formed, in which fracture occurs.

Grain refinement, an increase in the linear density of twin boundaries and the formation of deformation martensite all contribute to a significant increase in the strength characteristics of the steel. However, there is a high tendency to macroscopic localization of deformation, which is typical for steels with highly defective grain/subgrain structures of a submicron scale [36]. Despite the differences in the microstructure of the specimens treated in different modes of chemical-deformation processing, no principal differences are found in the mechanical properties of the specimens rolled to the same reduction. Nevertheless, hydrogen saturated and deformed with cooling specimens possess the highest mechanical properties (Table 3).

## Conclusions

Chemical-deformation processing of austenitic stainless Fe-17Cr-13Ni-3Mo-0.01C steel in rolling combined with hydrogen saturation provides the formation of a highly defective grain/subgrain structure. The deformation temperature and hydrogen saturation significantly affect the deformation mechanisms, phase transformations and final microstructure of the specimens in rolling.

Preliminary hydrogen saturation and decrease in deformation temperature (due to cooling of specimens before each rolling path) promote mechanical twinning and phase transformations during rolling of the specimens. Despite the formation of a small fraction of  $\epsilon$  and  $\alpha'$  martensitic phases in the structure, the main deformation mechanisms of the steel during rolling are slip, twinning, and microlocalization of plastic flow, which all assist the formation of the ultrafine-grained structures with various morphologies.

Grain refinement, accumulation of the defects of the crystal structure and the increase in internal stresses lead to an increase in the strength characteristics of the steel. Despite the fact that preliminary hydrogen saturation and decrease in temperature significantly affect the morphology of grain/subgrain structure and defective microstructure formed by rolling, they do not cause the significant hardening and plasticity loss of the specimens relative to those rolled at room temperature without preliminary saturation with hydrogen.

## References

1. Takeichi N., Senoh H., Yokota T., Tsuruta H., Hamada K., Takeshita H.T., Tanaka H., Kiyobayashi T., Takano T., Kuriyama N. "Hybrid hydrogen storage vessel", a novel high pressure hydrogen storage vessel combined with hydrogen storage material. *International Journal of Hydrogen Energy*, 2003, vol. 28, iss. 10, pp. 1121–1129. DOI: 10.1016/S0360-3199(02)00216-1.
2. Duschek D., Wellnitz J. High pressure hydrogen storage system based on new hybrid concept. *Sustainable Automotive Technologies*. Cham, 2013, pp. 27–33. DOI: 10.1007/978-3-319-01884-3\_3.
3. Macadre A., Artamonova M., Matsuoka S., Furtado J. Effects of hydrogen pressure and test frequency on fatigue crack growth properties of Ni-Cr-Mo steel candidate for a storage cylinder of a 70 MPa hydrogen filling station. *Engineering Fracture Mechanics*, 2011, vol. 78, iss. 18, pp. 3196–3211. DOI: 10.1016/j.engfracmech.2011.09.007.
4. Michler T., Marchi C.S., Naumann J., Weber S., Martin M. Hydrogen environment embrittlement of stable austenitic steels. *International Journal of Hydrogen Energy*, 2012, vol. 37, pp. 16231–16246. DOI: 10.1016/j.ijhydene.2012.08.071.
5. Perng T.P., Altstetter C.J. Comparison of hydrogen gas embrittlement of austenitic and ferritic stainless steels. *Metallurgical Transactions A*, 1987, vol. 18, pp. 123–134. DOI: 10.1007/BF02646229.
6. Shakhova I., Dudko V., Belyakov A., Tsuzaki K., Kaibyshev R. Effect of large strain cold rolling and subsequent annealing on microstructure and mechanical properties of an austenitic stainless steel. *Materials Science and Engineering: A*, 2012, vol. 545, pp. 176–186. DOI: 10.1016/j.msea.2012.02.101.
7. Wasnik D.N., Gopalakrishnan I.K., Yakhmi J.V., Kain V., Samajdar I. Cold rolled texture and microstructure in types 304 and 316L austenitic stainless steels. *ISIJ International*, 2003, vol. 43, no. 10, pp. 1581–1589. DOI: 10.2355/isijinternational.43.1581.



8. Padilha A.F., Plaut R.L., Rios P.R. Annealing of cold-worked austenitic stainless steels. *ISIJ International*, 2003, vol. 43, no. 2, pp. 135–143. DOI: 10.2355/isijinternational.43.135.
9. Ghosh S.K., Mallick P., Chattopadhyay P.P. Effect of cold deformation on phase evolution and mechanical properties in an austenitic stainless steel for structural and safety applications. *Journal of Iron and Steel Research International*, 2012, vol. 19, no. 4, pp. 63–68. DOI: 10.1016/s1006-706x(12)60089-2.
10. Ren-bo S., Jian-ying X., Dong-po H. Characteristics of mechanical properties and microstructure for 316L austenitic stainless steel. *Journal of Iron and Steel Research International*, 2011, vol. 18, no. 11, pp. 53–59. DOI: 10.1016/S1006-706X(11)60117-9.
11. Litovchenko I.Yu., Shevchenko N.V., Tyumentsev A.N., Naiden E.P. Fazovyi sostav i defektnaya substruktura austenitnoi stali 02X17T14M2 posle deformatsii prokatkoi pri komnatnoi temperature [Phase composition and defective substructure of austenitic steel 02Cr17Ni14Mo2 after room temperature rolling]. *Fizicheskaya mezomekhanika = Physical mesomechanics*, 2006, vol. 9, spec. iss. 1, pp. 137–140. DOI: 10.24411/1683-805X-2006-00050.
12. Litovchenko I.Yu., Tyumentsev A.N., Naiden E.P. Osobennosti martensitnykh prevrashchenii i evolyutsiya defektnoi mikrostruktury v protsesse prokatki metastabil'noi austenitnoi stali pri komnatnoi temperature [Peculiarities of martensite transformations and evolution of defect microstructure in metastable austenitic steel rolled at room temperature]. *Fizicheskaya mezomekhanika = Physical mesomechanics*, 2014, vol. 17, no. 1, pp. 31–42. DOI: 10.24411/1683-805X-2014-00045.
13. Hadji M., Badji R. Microstructure and mechanical properties of austenitic stainless steels after cold rolling. *Journal of Materials Engineering and Performance*, 2002, vol. 11, pp. 145–151. DOI: 10.1361/105994902770344204.
14. Eliezer D., Chakrapani D.G., Altstetter C.J., Pugh E.N. The influence of austenite stability on the hydrogen embrittlement and stress-corrosion cracking of stainless steel. *Metallurgical Transactions A*, 1979, vol. 10, pp. 935–941. DOI: 10.1007/BF02658313.
15. Singh S., Altstetter C. Effects of hydrogen concentration on slow crack growth in stainless steels. *Metallurgical Transactions A*, 1982, vol. 13, pp. 1799–1808. DOI: 10.1007/BF02647836.
16. Rozenak P., Bergman R. X-ray phase analysis of martensitic transformations in austenitic stainless steels electrochemically charged with hydrogen. *Materials Science and Engineering A*, 2006, vol. 437, pp. 366–378. DOI: 10.1016/j.msea.2006.07.140.
17. Yang Q., Luo J.L. Martensite transformation and surface cracking of hydrogen charged and outgassed type 304 stainless steel. *Materials Science and Engineering: A*, 2000, vol. 288, iss. 1, pp. 75–83. DOI: 10.1016/S0921-5093(00)00833-9.
18. Hoelzel M., Danilkin S.A., Ehrenberg H., Toebbens D.M., Udovic T.J., Fuessa H., Wipf H. Effects of high-pressure hydrogen charging on the structure of austenitic stainless steels. *Materials Science and Engineering: A*, 2004, vol. 384, iss. 1–2, pp. 255–261. DOI: 10.1016/j.msea.2004.06.017.
19. Schramm R., Reed R. Stacking fault energies of seven commercial austenitic stainless steels. *Metallurgical Transactions A*, 1975, vol. 6, pp. 1345–1351. DOI: 10.1007/bf02641927.
20. Rhodes C., Thompson A. The composition dependence of stacking fault energy in austenitic stainless steels. *Metallurgical Transactions A*, 1977, vol. 8, pp. 1901–1906. DOI: 10.1007/BF02646563.
21. Piatti G., Schiller P. Thermal and mechanical properties of the Cr-Mn-(Ni-free) austenitic steels for fusion reactor applications. *Journal of Nuclear Materials*, 1986, vol. 141–143, pp. 417–426. DOI: 10.1016/S0022-3115(86)80076-9.
22. Qi-Xun D., Xiao-Nong W., Cheng A.-D., Xin-Min L., Xin-Min L. Stacking fault energy of cryogenic austenitic steels. *Chinese Physics*, 2002, vol. 11, no. 6, pp. 596–600. DOI: 10.1088/1009-1963/11/6/315.
23. Koyama M., Akiyama E., Sawaguchi T., Ogawa K., Kireeva I.V., Chumlyakov Yu.I., Tsuzaki K. Hydrogen-assisted quasi-cleavage fracture in a single crystalline type 316 austenitic stainless steel. *Corrosion Science*, 2013, vol. 75, pp. 345–353. DOI: 10.1016/j.corsci.2013.06.018.
24. Melnikov E., Maier G., Moskvina V., Astafurova E. Structure, phase composition and mechanical properties of austenitic steel Fe–18Cr–9Ni–0.5Ti–0.08C subjected to chemical deformation processing. *AIP Conference Proceedings*, 2016, vol. 1783, pp. 020151-1 – 020151-4. DOI: 10.1063/1.4966444.
25. Melnikov E., Maier G., Moskvina V., Astafurova E. Influence of hydrogenation regime on structure, phase composition and mechanical properties of Fe18Cr9Ni0.5Ti0.08C steel in cold rolling. *AIP Conference Proceedings*, 2017, vol. 1909, pp. 020136-1 – 020136-4. DOI: 10.1063/1.5013817.
26. Kreslin V.Y., Naiden E.P. Automatic complex for a study of the characteristics of hard magnetic materials. *Instruments and Experimental Techniques*, 2002, vol. 45, pp. 55–57. DOI: 10.1023/A:1014548225622. Translated from *Pribory i tekhnika eksperimenta*, 2002, no. 1, pp. 83–86.



27. Utevskii L.M. *Difraktsionnaya elektronnyaya mikroskopiya v metallovedenii* [Diffraction electron microscopy in metal science]. Moscow, Metallurgiya Publ., 1973. 584 p.
28. Christian J.W., Mahajan S. Deformation twinning. *Progress in Materials Science*, 1995, vol. 39, no. 1–2, pp. 1–157. DOI: 10.1016/0079-6425(94)00007-7.
29. Sathiyamoorthi P., Asghari-Rad P., Karthik G.M., Zargarani A., Kim H.S. Unusual strain-induced martensite and absence of conventional grain refinement in twinning induced plasticity high-entropy alloy processed by high-pressure torsion. *Materials Science and Engineering: A*, 2021, vol. 803, p. 140570. DOI: 10.1016/j.msea.2020.140570.
30. Astafurova E.G., Tukeeva M.S., Maier G.G., Melnikov E.V., Maier H.J. Microstructure and mechanical response of single-crystalline high-manganese austenitic steels under high-pressure torsion: The effect of stacking-fault energy. *Materials Science and Engineering: A*, 2014, vol. 604, pp. 166–175. DOI: 10.1016/j.msea.2014.03.029.
31. Kireeva I.V., Chumlyakov Yu.I., Luzginova N.V. Skol'zhenie i dvoynikovanie v monokristallakh austenitnykh nerzhavayushchikh staley s azotom [Slip and twinning in single crystals of austenitic stainless steels with nitrogen]. *Fizika metallov i metallovedenie = The Physics of Metals and Metallography*, 2002, vol. 94, no. 5, pp. 92–104. (In Russian).
32. Litvinova E.I., Kireeva I.V., Zakharova E.G., Luzginova N.V., Chumlyakov Yu.I., Sekhitoglu Kh., Karaman I. Dvoynikovanie v monokristallakh stali Gadfil'da [Twinning of Hadfield steel single crystals]. *Fizicheskaya mezomekhanika = Physical mesomechanics*, 1999, vol. 7 (1–2), pp. 115–121.
33. Shul'mina A.A., Luzginova N.V., Kireeva I.V., Chumlyakov Yu.I., Ul'yanycheva V.F. Mekhanizmy deformatsii monokristallov austenitnykh nerzhavayushchikh staley, legirovannykh azotom [Deformation mechanisms of austenitic stainless steel single crystals alloyed with nitrogen]. *Fizicheskaya mezomekhanika = Physical mesomechanics*, 2004, vol. 7, spec. iss., pt. 1, pp. 253–265.
34. Astafurova E.G., Zakharova G.G., Maier H.J. Hydrogen-induced twinning in  $\langle 001 \rangle$  Hadfield steel single crystals. *Scripta Materialia*, 2010, vol. 63, iss. 12, pp. 1189–1192. DOI: 10.1016/j.scriptamat.2010.08.029.
35. Astafurova E.G., Maier G.G., Melnikov E.V., Moskvina V., Vojtsik V., Zakharov G., Smirnov A., Bataev V. Effect of hydrogen charging on mechanical twinning, strain hardening, and fracture of  $\langle 111 \rangle$  and  $\langle 144 \rangle$  hadfield steel single crystals. *Physical Mesomechanics*, 2018, vol. 21, pp. 263–273. DOI: 10.1134/S1029959918030116.
36. Kozlov E.V., Glezer A.M., Koneva N.A., Popova N.A., Kurzina I.A. *Osnovy plasticheskoi deformatsii nanostrukturnykh materialov* [Fundamentals of plastic deformation of nanostructured materials]. Moscow, Fizmatlit Publ., 2016. 304 p. ISBN 978-5-9221-1689-3.

## Conflicts of Interest

The authors declare no conflict of interest.

© 2021 The Authors. Published by Novosibirsk State Technical University. This is an open access article under the CC BY license (<http://creativecommons.org/licenses/by/4.0/>).